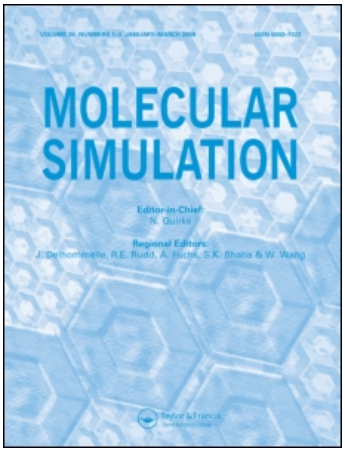

Molecular Simulation

Publication details, including instructions for authors and subscription information:
http://www.informaworld.com/smpp/title~content=t713644482

Interaction between a twelve-residue segment of antifreeze protein type I, or its mutants, and water molecules

Takashi Nobekawa[a]; Hiromi Taniguchi[a]; Yoshimichi Hagiwara[a]
[a] Department of Mechanical and System Engineering, Graduate School of Science and Technology, Kyoto Institute of Technology, Kyoto, Japan

To cite this Article Nobekawa, Takashi , Taniguchi, Hiromi and Hagiwara, Yoshimichi(2008) 'Interaction between a twelve-residue segment of antifreeze protein type I, or its mutants, and water molecules', Molecular Simulation, 34: 3, 309 — 325
To link to this Article: DOI: 10.1080/08927020701830219
URL: http://dx.doi.org/10.1080/08927020701830219

Molecular Simulation
Vol. 34, No. 3, March 2008, 309–325

Taylor & Francis
Taylor & Francis Group

Interaction between a twelve-residue segment of antifreeze protein type I, or its mutants, and water molecules

Takashi Nobekawa, Hiromi Taniguchi and Yoshimichi Hagiwara*

Department of Mechanical and System Engineering, Graduate School of Science and Technology, Kyoto Institute of Technology, Kyoto, Japan

(Received 14 April 2007; final version received 24 November 2007)

A molecular dynamics simulation has been carried out for water molecules with a rigid segment of antifreeze protein type I. The segment consists of nine alanine residues, two threonine residues and one asparagine residue. Mutant segments, in which the threonine residues are replaced with valine residues, or serine residues, are also used. It is predicted that the hydrogen site of asparagine residue, and that of threonine residue, play an important role in the hydrogen bond of water molecules in these sites. This hydrogen bond is not noticeable between water molecules and the valine residue, or serine residue. The existence of four hydrophilic sites enhances the mobility of water molecules close to the serine residue of the mutant segment. The difference in the zenith-angle fluctuations of the original segment and the valine-mutant segment is less noticeable in the case of 230 K. This is because the gathering of water molecules due to the hydrophobic hydration is predominant near the alanine residues of the segments at this temperature.

Keywords: antifreeze protein type I; segments; valine mutant; serine mutant; angular distribution function

1. Introduction

Attention has recently been paid to the inhibition of ice crystal growth. According to Li and Sun [1], this inhibition is important for the development of new frozen foods and the improvement of the taste of these foods. This inhibition is also a key factor for developing freeze-resistant fish for aquaculture, or producing cold–hardy varieties of plants for agriculture as was reported by Fletcher *et al*. [2]. Furthermore, it is important for the low-temperature preservation of organs, which are to be transplanted, according to Amir *et al*. [3].

Various methods have been proposed for the inhibition. One of the most promising methods is the use of a non-toxic additive, which has the function of lowering the freezing point while retaining the melting point. The growth of ice can be inhibited easily by keeping the preservation temperature in the range between the two temperatures. Although sodium chloride and alpha-linked sugar (Trehalose) are known to lower the freezing point, these also lower the melting point. Antifreeze proteins (AFPs) are appropriate additives because they are non-toxic and they cause a wide gap between the freezing point and melting point. Furthermore, the AFPs do not increase osmotic pressure.

Among many AFPs discovered so far, HPLC6, which is one of the major components of AFP type I and is extracted from winter flounder, has been focused on in many studies. Yang *et al*. [4] clarified from the analysis of its X-ray crystallographic structure that the HPLC6 consists of 37 residues of amino acids and forms α-helix. More than two thirds of these residues are hydrophobic alanine residues. Four hydrophilic threonine residues (Thr2, Thr13, Thr24 and Thr35) are on one side of the helix at nearly identical distances.

The following hypothesis of the antifreeze mechanism has been accepted: the hydrogen atoms of the hydroxyl sites of the threonine residues are bonded to the oxygen atoms on the pyramidal plane of $(20\bar{2}1)$ in the ice *Ih* crystal, because the distance of the hydrogen atoms is nearly equal to the repetitive distance of the oxygen atoms along the direction of $(10\bar{1}2)$ on the plane (See Knight *et al*. [5]). Consequently, many alanine residues orient themselves away from the ice surface and interfere with the approach of water molecules to the surface (See, for example, Ye and Feeney [6]). This is consistent with the experimental results, in which only bi-pyramidal ice crystals were observed in the solution of the HPLC6 at subzero degrees, obtained by Chao *et al*. [7] and Zhang and Laursen [8].

However, experimental results inconsistent with this hypothesis have been obtained recently by using mutants of HPLC6. Table 1 shows typical mutants adopted by Chao *et al*. [7], Zhang and Laursen [8], Haymet *et al*. [9] and Loewen *et al*. [10]. The ratio of the thermal hysteresis of each mutant in the case of its concentration of 5 mg/ml to that of HPLC6 is also indicated in the table. In addition, the growth of an ice crystal, whose shape is

*Corresponding author. Email: yoshi@kit.ac.jp

ISSN 0892-7022 print/ISSN 1029-0435 online

DOI: 10.1080/08927020701830219
http://www.informaworld.com

Table 1. Comparison of mutants of HPLC6.

	Residues of mutants						Ratio of thermal hystereses	Ice growth
HPLC6	Thr2	Thr13	Asn16	Thr24	Asn26	Thr35	1	No
Chao [7]	Thr	Val	Asn	Val	Asn	Thr	0.86	No
Zhang [8]	Val	Val	Asn	Val	Asn	Val	0.33	Gradual
Haymet [9]	Val	Val	Asn	Val	Asn	Val	0.85	No
Chao [7]	Thr	Ser	Asn	Ser	Asn	Thr	0.14	Yes
Zhang [8]	Thr	Ser	Asn	Thr	Asn	Thr	0.90	No
	Thr	Thr	Asn	Ser	Asn	Thr	0.72	No
	Ser	Thr	Asn	Thr	Asn	Ser	0.68	No
	Ser	Thr	Asn	Ser	Asn	Ser	0	Yes
	Ser	Ser	Asn	Ser	Asn	Ser	0	Yes
Loewen [10]	Thr	Thr	Thr	Thr	Thr	Thr	1.09	No
	Thr	Thr	Val	Thr	Val	Thr	0.63	No
	Thr	Thr	Gln	Thr	Gln	Thr	0	–

hexagonal bipyramid or trapezohedron, is summarised in the table. It is found from the table that the hydroxyl groups and methyl groups in the threonine residues can contribute to the antifreeze activity, as Zhang and Laursen [8] and Jorov *et al*. [11] pointed out. Furthermore, the location of atoms in the sites of asparagine residue (Asn27) also contributes to the antifreeze activity.

In order to investigate the roles of residues in more detail, many molecular dynamics studies have been carried out. Cheng and Merz [12] noted that both the hydrogen bond and van der Waals' interaction play an important role in the binding of protein onto the ice surface. They also mentioned that hydrophobic interactions might be important. Dalal *et al*. [13] investigated the effect of the HPLC6 molecule on the water molecules in the liquid phase near the pyramidal plane of the ice crystal. They concluded that there is no gain in hydrogen bonds when interaction occurs between the proteins and the ice/water interface. Yang and Sharp [14] found that the mutant, in which the threonine residues are replaced with hydrophilic serine residue, causes a polar-like hydration. Nevertheless, the interactions between water molecules and the sites of amino acid residues in the HPLC6, or in its mutant, have not yet been clarified.

Most of the molecular dynamics analyses mentioned above handled the adsorbed HPLC6 on the ice pyramidal plane. The present authors consider that these analyses predict the latter stage of the whole antifreeze activity of HPLC6. However, the early stage of the whole activity, when the HPLC6 is about to interact with an ice surface, has not yet been clarified. This early stage may occur in the blood flow in the capillary of winter flounder. In this case, the thermal state is not equilibrium and quite low heat flux exists. These thermal conditions are not the same as those in the crystal growth tests conducted by Chao *et al*. [7], Zhang and Laursen [8], Haymet *et al*. [9] and Loewen *et al*. [10], but similar to those in the crystal habit tests (or the one-dimensional ice growth test in a narrow gap) conducted by Haymet *et al*. [15] and Coger *et al*. [16]. When the concentration of AFP and the growth rate of ice (and thus heat flux) are low, only prism faces are observed in the crystal habit test (See Coger *et al*. [16]). When the concentration of AFP and the growth rate of ice are high, not only prism faces but also pyramidal planes (not necessarily the $(20\bar{2}1)$ planes) are observed. Furthermore, the images of ice surfaces suggest that the pyramidal planes are formed from the edge of the prism faces. Therefore, it is worth analysing the interactions among the prism faces of ice, HPLC6 and surrounding water in order to elucidate the formation mechanism of bipyramidal ice crystals.

We have carried out molecular dynamics simulations on the mixture of water, an ice nucleus and the models of HPLC6. The goal of our study is to elucidate the early stage of the interaction between the HPLC6 and a growing ice nucleus, which may appear in winter flounder. In the first step, we carry out a molecular dynamics simulation of water molecules in a liquid phase with a segment of HPLC6 or its mutants. In the mutant segment, the threonine residues in the original segment are replaced with valine residues, or serine residues. We discuss the statistics of the water molecules affected by the segments. The interaction between the segments and an ice crystal will be discussed in the next paper [17].

2. Simulation procedures

2.1 Assumptions

The number of molecules, the volume of the simulation domain and the total energy were kept constant except for the period of the temperature scaling mentioned below. All the water molecules were assumed to be rigid bodies. The net dipole moment was not evaluated. The periodic boundary condition was imposed on the computational domain.

2.2 Governing equations

The Newton–Euler equations for the translational and rotational motions of the molecules were solved at each time step, and were integrated with time by using the Gear algorithm [18]. We used a 5-value Gear algorithm, in which the time derivatives up to the fifth order were considered, to the Newton equation for the translational motion. We adopted a 4-value Gear algorithm to the Euler equation for the rotation. All the computations were carried out with the time step of 0.5 fs.

2.3 Temperature adjustment

The statistical temperature, T, was given by the total energy of the translational motion for all the molecules, K_T and that of the rotational motion for the molecules, K_R. The temperature is expressed as follows:

$$T = \frac{1}{2}\left(\frac{2}{3k_B N}K_T + \frac{2}{3k_B N}K_R\right) = \frac{1}{3k_B N}\left(\frac{1}{2}\sum_{i=1}^{N} m\mathbf{v}_i^2 + \frac{1}{2}\sum_{i=1}^{N}\left(I_{px_i}\omega_{px_i}^2 + I_{py_i}\omega_{py_i}^2 + I_{pz_i}\omega_{pz_i}^2\right)\right) \quad (1)$$

where k_B is the Boltzmann constant, N is the total number of molecules, m is the mass of molecules and I_p is the inertia moment based on its principal axis. In order to obtain supercooled water, temperature scaling was carried out, in which the translational velocity, $\mathbf{v}$, and the angular velocity, ω, of each molecule were changed by the following equation:

$$\mathbf{v}_i^{(new)} = \mathbf{v}_i^{(old)}\sqrt{\frac{T_{pd}}{T}}, \quad \omega_i^{(new)} = \omega_i^{(old)}\sqrt{\frac{T_{pd}}{T}} \quad (2)$$

where T_{pd} is the predetermined temperature. The predetermined temperatures were 300 K (Case 1) and 230 K (Case 2).

2.4 Potential functions of water molecules

The TIP4P potential proposed by Jorgensen *et al*. [19] was used for the potential function for the interaction between two water molecules. This potential function consists of the Coulomb potential and the Lennard-Jones potential. In order to reduce the force of far distant molecules, a cutoff radius was set for the Lennard-Jones potential, and the Ewald method (See Frenkel and Smit [20]) was used for the Coulomb potential. Since we applied the group-based cutoff to this procedure, the cutoff radius of the atom group was measured from an indicator point of the group. This point was arranged at the centre of mass of each water molecule. The cutoff radius was 1.2 nm. The parameters for the Ewald summation were $\alpha = 10.6$, $|\mathbf{u}|_{max} = 1$, $|\mathbf{h}|^2_{max} = 27$, where α is the width of the Gaussian distribution, $\mathbf{u}$ is the vector for the location of the image cell in the physical space and $\mathbf{h}$ is the vector for the location of the image cell in the Fourier space. In order to reduce the computational time, we adopted the method of non-bonded neighbour list proposed by Verlet [21].

2.5 Segment of HPLC6

Figure 1(a) shows the segment of AFP type I adopted in the present study (TT segment). This segment consists of 12 amino acid residues. The sequence of these residues represents that of the HPLC6, namely Thr24, Ala25, Ala26, Asn27, Ala28, Ala29, Ala30, Ala31, Ala32, Ala33, Ala34 and Thr35. Although the segment has the disadvantage in that the effect of other amino acid residues of the HPLC6 on the segment cannot be considered, it has the advantages in that the effect of hydrophilic residues can be highlighted and that the segment is small enough to obtain reliable statistics concerning the interaction between the segment and surrounding water molecules. Each methyl site is replaced with a single atom for simplicity. The atom group of CO—NH—CH_3 is connected to the other side of the alanine residue of each threonine residue in order to reduce the terminus effect on the threonine residues. The atoms in these groups are surrounded with broken lines in the figure. Hereafter, the hydrogen site far from the helical axis in the amino group of Asn27 is designated as H_{N1}, and the other hydrogen site is designated as H_{N2} in order to discuss the hydrogen bond between these hydrogen sites and the oxygen atoms of water molecules.

Figure 1(b) indicates the TT segment viewed along the axis. In the α-helical conformation, 3.6 residues exist per turn. The pitch of turn along the axis is 0.54 nm. In order to make the discussion clear, we divide the segment into two sides: 'the hydrophobic side', in which only the alanine residues (Ala25, Ala26, Ala29, Ala30, Ala32 and Ala33) are included, and 'the hydrophilic side', in which the other residues (Thr24, Asn27, Ala28, Ala31, Ala34 and Thr35) are included. This classification is different from the three-side classification proposed by Jorov *et al*. [11]. This is because our segments do not contain the four residues (Ser4, Lvs18, Glu22 and Arg37), which form the boundary between the hydrophobic side and hydrophilic side in their classification.

We made one mutant segment (VV segment) from the TT segment by replacing the hydroxyl group in the two threonine residues with the methyl site. Similarly, we made another mutant segment (SS segment) from the TT segment by replacing the methyl site in the threonine residues with the hydrogen atom.

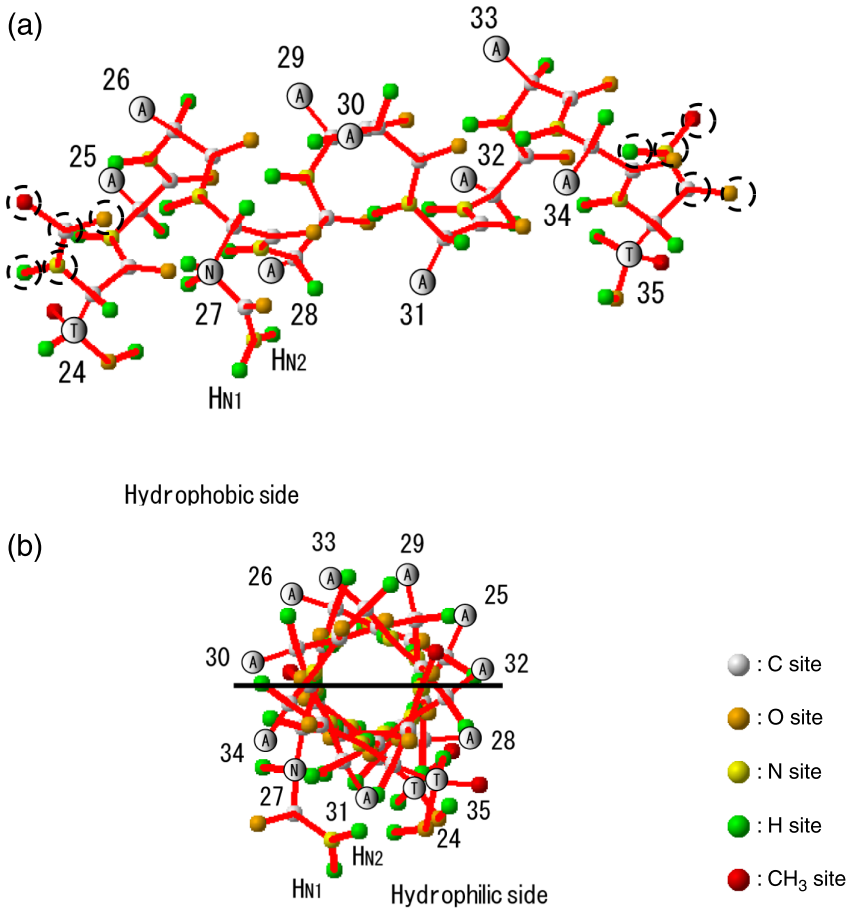

Figure 1. TT segment: (a) view from side, (b) view from the helical axis.

The dihedral angles of the peptide bond, φ and ψ, were retained at $-57°$ and $-48°$, respectively, based on the angles of an ideal α-helix described by Cheng and Merz [12]. Thus, the segment conformation was unchanged through the computation. This rigidness can be considered as an overestimation of the hydrogen bond between two adjacent sites in the axial direction of the segments. Flexibility can be considered by adopting an algorithm, such as SHAKE (See Ryckart *et al.* [22]). However, we did not include any algorithm for the flexibility because the time constants of the deformation of AFPs are not clear. In addition, the fluctuation of the dihedral angles is within nine degrees for the central residues of HPLC6 in the molecular dynamics simulation when using AMBER, according to Cheng and Merz [12]. Thus, the rigid segments are not too unrealistic. The dihedral angles of sites of the atom group in the residues were also determined from the angles in the table illustrated by Cheng and Merz [12].

The OPLS parameters developed by Jorgensen *et al.* [23] were adopted as the potential parameters of each site of the segments. The electric charge was defined for the methyl site in one end (C-terminus connected to Thr24, Val24 or Ser24) so that the sums of the electric charges of the segments were zero. The cutoff radius was 1.5 nm. The indicator point for the radius was allocated at the centre of each group in the segment where the electric charge was zero (See Reach [24]). The parameters for the Ewald summation of the water–water interaction were used for the parameters for the summation of the water–site interaction.

2.6 *Computational conditions*

The total number of water molecules and the dimension of computational domain in Cases 1 and 2 are shown in Table 2. The dimension is the same as that adopted in our previous study [25]. We will deal with hexagonal ice crystals, whose prism faces have dimensions of 1.04×3.03 and $1.81 \times 3.76\,\mathrm{nm}^2$, in the next paper [17]. The segments are not too small to consider the statistics for the interaction between the sites of the segments and the water molecules adjacent to these faces.

A number of water molecules were removed from the central part of the domain in order to form a cocoon-shaped void. The segment was introduced into this void.

Table 2. Computational condition.

	Case 1	Case 2
Number of water molecules	2843	2836 (2837*)
Computational domain (nm)	4.667 × 4.491 × 4.400	
Density (g/cm^3)	0.922	

* Only in the case with the VV segment.

The z axis was positioned along the helical axis of the segment. Then, the x axis was positioned from the hydrophobic side of the segment to the hydrophilic side.

The scaling of temperature and velocity was carried out for 190 ps as shown in Table 3. The procedure was the same as that explained in our previous study [25].

3. Statistical quantities

We dealt with the following five functions for the discussion. These functions were obtained from the result in the period of 190–240 ps unless denoted.

3.1 Mean square displacement

The mean square displacement (MSD) of molecules, $D(t)$, is defined by the following equation:

$$D(t) = \frac{1}{N}\left\langle \sum_j \left|\mathbf{r}_j(t_0 + t) - \mathbf{r}_j(t_0)\right|^2 \right\rangle \tag{3}$$

where $\mathbf{r}_j$ is the position vector of a molecular j, t is time, t_0 is a reference time, N is the number of molecules and the angle bracket shows a time mean value. The value of the MSD indicates how easily the molecules diffuse. The time dependency of the MSD indicates whether the system is in a solid, liquid or gas phase. If the system is in thermal equilibrium, the value of the MSD and its time dependency do not depend on the reference time. The MSD of water molecules was calculated from the position vectors for the periods of 10 ps at an interval of 0.25 ps (i.e. the periods of 190–200, 190.25–200.25, 190.5–200.5, ..., 230–240 ps). The moving-averaged values of the MSD will be discussed later.

3.2 Correlation function of rotation

The rotational motions of each water molecule are investigated using the correlation function of rotation, $C_R(t)$ (CFR). The CFR can be experimentally obtained from Raman scattering, or NMR (Nuclear Magnetic Resonance). The CFR is defined by the following equation:

$$C_R(t) = \frac{1}{2N}\left\langle \sum_j \left[3\left\{\mathbf{u}_j(t_0 + t) - \mathbf{u}_j(t_0)\right\}^2 - 1\right] \right\rangle$$
$$= \frac{1}{2N}\left\langle \sum_j \left[3\cos^2\theta_j(t) - 1\right] \right\rangle \tag{4}$$

where $\mathbf{u}_j(t_0)$ is the unit vector of one O—H axis in a molecule j at t_0 and $\theta_j(t)$ is the angle between $\mathbf{u}_j(t_0 + t)$ and $\mathbf{u}_j(t_0)$. If the rotational motion is retained, the randomness of the motion is reduced. In this case, the CFR keeps high values. The CFR of water molecules was calculated from the unit vectors for the periods of 10 ps at an interval of 0.25 ps (i.e. the periods of 190–200, 190.25–200.25, 190.5–200.5, ... 230–240 ps). The moving-averaged values of the CFR will be discussed later.

3.3 Radial distribution function

The radial distribution function (RDF) between an atom of water molecule or a site of the segments and oxygen atoms in a spherical shell is defined as follows (See, for example, Allen and Tildesley [26]):

$$g(r) = \frac{V}{4\pi r^2 \Delta r N^2}\left\langle \sum_i \sum_{j \neq i} \delta(\mathbf{r}_i - \mathbf{r}_j) \right\rangle, \tag{5}$$

where $r = |\mathbf{r}_i - \mathbf{r}_j|$ is the distance between two atoms (or between a site and an atom), V is the volume of

Table 3. Duration of computation.

	Period [ps]	Water molecules	Segments	Predetermined temperature T_{pd} [K] Case 1	Case 2
Scaling procedure	0–30	Free	Fix	300	230
	30–60	Free	0.1%**	300	230
	60–90	Free	Free	300	230
	90–190	Free	Free	Free	Free
Sampling procedure*	190–240	Free	Free	Free	Free

* The moving average is adopted for MSD and CFR. ** The displacement is reduced to 0.1% of its predicted value.

computational domain, Δr is the thickness of the shell, N is the number of oxygen atoms and δ is the delta function. Δr was equal to 0.01 nm.

3.4 Angular distribution function

Yang and Sharp [14] discussed the water–water angle θ shown in Figure 2(a). A typical example of the probability distribution of θ in our simulation is shown in Figure 2(b). This is similar to the results obtained by Yang and Sharp. The distribution is effective for estimating the overall hydrogen bond between water molecules. However, the distribution depends on the distance between two molecules. Furthermore, the definition of θ is not sufficient for considering the hydrogen bond between oxygen atom or hydrogen atom in the residues and water molecules.

Here, we introduce a new function of both the angle α_{HB} and distance r. This angle is defined by the two lines as follows: the first line passes through the atom (or the site) at the shell centre and an oxygen atom inside the shell. The second line is along the covalent bond between the oxygen atom inside the shell and the hydrogen atom located at a farther distance than the other hydrogen atom, when the oxygen atom of a water molecule is at the shell centre as shown in Figure 3(a). (Hereafter, the solid line and dotted line between any two atoms represent the covalent bond and hydrogen bond, respectively.) The relationship between the α_{HB} and the water–water angle is given by the following equation:

$$\theta = |\alpha_{HB} - \alpha_{HOH}| (0 \leq \theta \leq 180°\text{-}\alpha_{HOH}\ \text{degrees})$$

where α_{HOH} is the H—O—H angle of water molecules, and is equal to 104.52° for the TIP4P potential.

The other cases of the second line can be considered. The second line is along the covalent bond between the hydrogen atom at the shell centre and the oxygen atom, when one of the hydrogen atoms of a water molecule is at the shell centre, as shown in Figure 3(b). The angle shown in Figure 3(b) is useful for examining the hydrogen bond among several water molecules.

The definition of α_{HB} can be expanded in the case where an atom of the segments is located at the shell centre. The second line is along the covalent bond between the oxygen atom inside the shell and the hydrogen atom located at a farther distance than the other hydrogen atom, when the oxygen site or nitrogen site of a hydrophilic group of the segments is at the shell centre (Figure 3(c)). The second line is along the covalent bond between the hydrogen site and the oxygen site (or nitrogen site) of the hydrophilic group, when a hydrogen site of a hydrophilic group of the segments is at the shell centre (Figure 3(d)).

When a methyl site of the segments is at the shell centre, the second line is along the covalent bond between the oxygen atom and the hydrogen atom located at a farther distance from the methyl site than the other hydrogen atom, as shown in Figure 3(e). Also, the second line is along the covalent bond between the oxygen atom and the hydrogen atom located at a nearer distance from the methyl site than the other hydrogen atom, as shown in Figure 3(f).

The distribution function of α_{HB} is defined as follows:

$$A(r, \alpha_{HB}) = g(r) \frac{\sum n(r, \alpha_{HB})}{\sum_{\alpha_{HB}=0°}^{180°} \sum n(r, \alpha_{HB})} \qquad (6)$$

where n is the number of water molecules whose oxygen atoms are located inside the spherical shell mentioned above and form an angle of α_{HB} with the atom (or the site) at the shell centre. The RDF is multiplied in order to reduce the effect of an increase in the number of water molecules with the distance to the function. The function, $A(r, \alpha_{HB})$, is called the angular distribution function (ADF). The relationship between the ADF and the probability distribution of θ discussed by Yang and Sharp [14] is as follows:

$$P(\theta) = \int_0^{0.4\,\text{nm}} \frac{A(r, \alpha_{HB})}{g(r)} \mathrm{d}r.$$

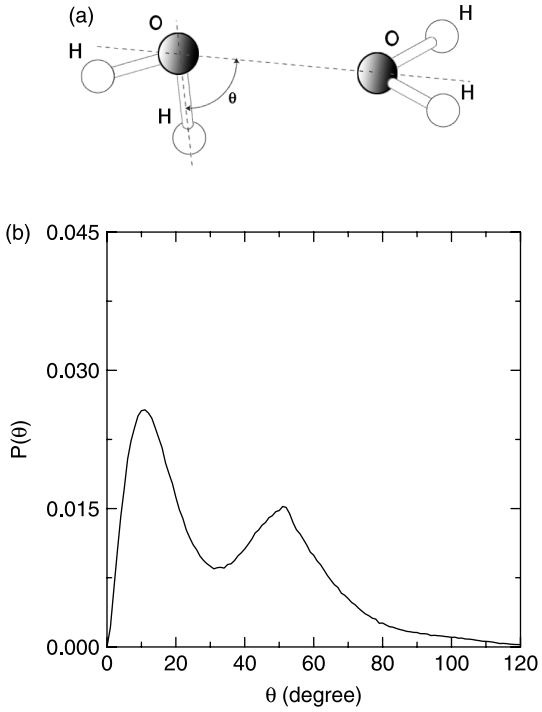

Figure 2. Water–water angle defined by Yang and Sharp: (a) definition, (b) typical probability distribution.

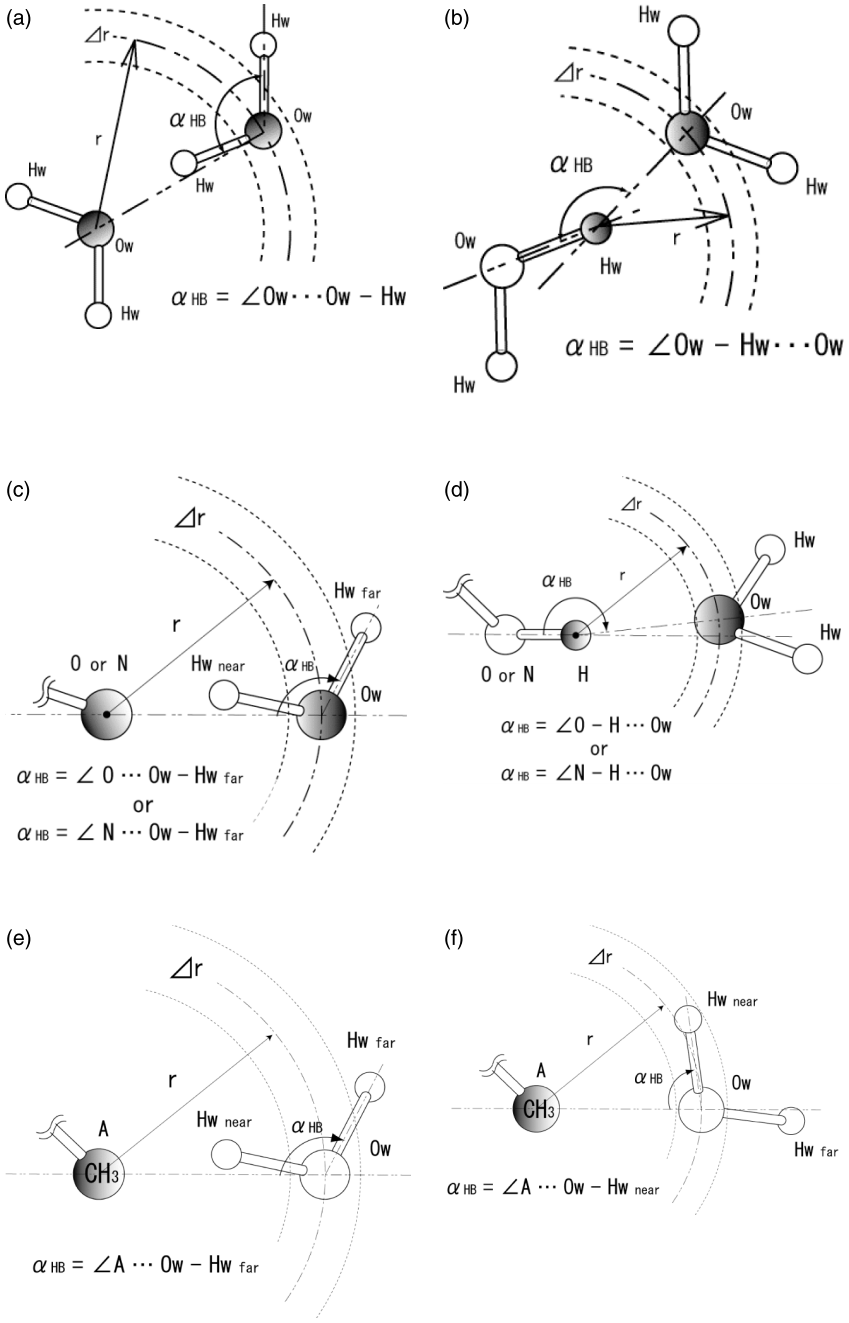

Figure 3. Angle of α_{HB} in the definition of ADF: (a) $O_w \cdots O_w$—$H_{w\ far}$, (b) O_w—$H_w \cdots O_w$, (c) O (or N) $\cdots$ O_w—$H_{w\ far}$, (d) O (or N)—H $\cdots$ O_w, (e) A (CH_3) $\cdots$ O_w—$H_{w\ far}$, (f) A (CH_3) $\cdots$ O_w—$H_{w\ near}$.

3.5 Dihedral angular distribution function

Since we replaced each methyl site with the single atom, we can specify the water molecules inside the first hydration shell of a methyl site by using the RDF of the site. Furthermore, we can examine the orientation of the specific water molecules by considering the dihedral angle, β, for the water molecules. Figure 4 indicates the dihedral angle of two planes defined by the three atoms of the water molecule and the methyl site. β is equal to 0° when all the atoms and the site are on a plane. The dihedral angular distribution function (DADF) is defined as follows:

$$T(r, \alpha_{HB}, \beta) = A(r, \alpha_{HB}) \frac{\sum n(r, \alpha_{HB}, \beta)}{\sum_{\beta} \sum n(r, \alpha_{HB}, \beta)}. \quad (7)$$

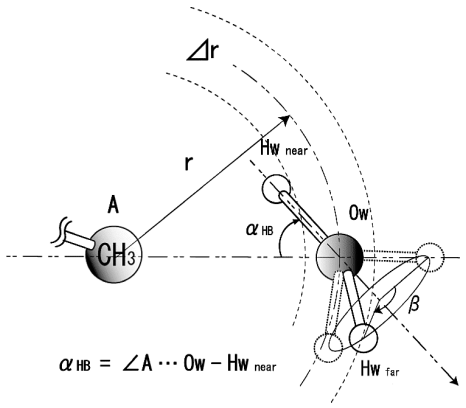

Figure 4. Dihedral angle of β in the definition of DADF.

4. Results and discussion

4.1 Zenith angle

Figure 5 depicts the time changes in the components of the zenith angle of the segment during the scaling period shown in Table 3. At the initial stage ($t = 0$ ps), the x component, γ_x and the y component, γ_y, were 90° and the z component, γ_z, was 0°. It is found that the deviation from the initial stage and the change of the zenith angle of the TT segment are more noticeable than those of the VV segment, respectively, at 300 K (Case 1). This suggests the interaction between the water molecules and the threonine residues is different from that between the water molecules and the valine residues. The differences in deviation from the initial stage and the change in the zenith angle due to the difference in the segment become small at 230 K (Case 2).

4.2 Mean displacement of water molecules

Figure 6(a) and (b) show the MSD of the water molecules at 300 K in the case with the TT segment, and in the case with the VV segment, respectively. Figure 6(c) and (d) show the MSD of the water molecules at 230 K in the case with the TT segment, and in the case with the VV segment, respectively. In these figures, $t = 0$ ps represents the initial instants of the MSDs for the periods of 10 ps (i.e. 190, 190.25, ..., 230 ps). Note that the displacement of the centre of mass of the segment has already been subtracted from the MSD. The solid lines indicate the results of the molecules whose distance from any site of the segments is shorter than 0.55 nm (hereafter called 'near TT' or 'near VV'). The broken lines in these figures indicate the results of the molecules whose distance from any site of the segments is longer than 0.55 nm (hereafter called 'far from TT' or 'far from VV'). The radius of the second hydration shell is 0.55 nm. It is found that the MSD of water molecules near the segments takes lower values compared with that far from the segments. Thus, the translational motion of water molecules is attenuated by the segments.

We confirmed that the moving-averaged MSD in the case of the TT segment for the period of 190–202.5 ps in Case 2 differs at most 8% from the MSD shown in Figure 6(c). This indicates that the impact of introduction of the segment into the void is negligible in the period of the sampling procedure.

Figure 6(e) exhibits the MSD of the water molecules in the case with the SS segment at 230 K. The MSD of the molecules near the SS segment is higher than those near the other segments. This shows that the water molecules near the serine residues diffuse more easily than the threonine or valine residue. This will be discussed later.

4.3 Rotation of water molecules

The CFR of the water molecules at 300 K in the case with the TT segment and that in the case with the VV segment are shown in Figure 7(a) and (b), respectively. The CFR of the water molecules at 230 K in the case with the TT segment, and in the case with the VV segment are indicated in Figure 7(c) and (d), respectively. In these figures, $t = 0$ ps represents the initial instants of the CFRs for the periods of 10 ps (i.e. 190, 190.25, ..., 230 ps). The line types are the same as those in Figure 6. It is found that the CFR of the molecules near the segment takes higher values compared with that far from the segment. Thus, the rotational motion of water molecules is retained in the vicinity of the TT segment. This shows that the TT segment reduces the randomness of the rotational motion of water molecules nearby. This is also obtained in the case with the VV segment.

We confirmed that the moving-averaged CFR in the case of the TT segment for the period of 190–202.5 ps in Case 2 differs at most 4% from the CFR shown in Figure 7(c). This indicates that the impact of introduction of the segment into the void is negligible in the period of the sampling procedure.

Figure 7(e) exhibits the CFR of the water molecules in the case with the SS segment at 230 K. The CFR of the molecules near the SS segment is lower than those near the other segments. Furthermore, these CFRs are lower than that for the molecules far from the SS segment. This clearly shows that the water molecules near the serine residues rotate more randomly than the molecules near the threonine or valine residue. This will be discussed later.

4.4 Angular distribution function

4.4.1 In the case without segment

Figure 8 indicates the ADF of water molecules at 300 K in the case without the segment. A peak is seen around

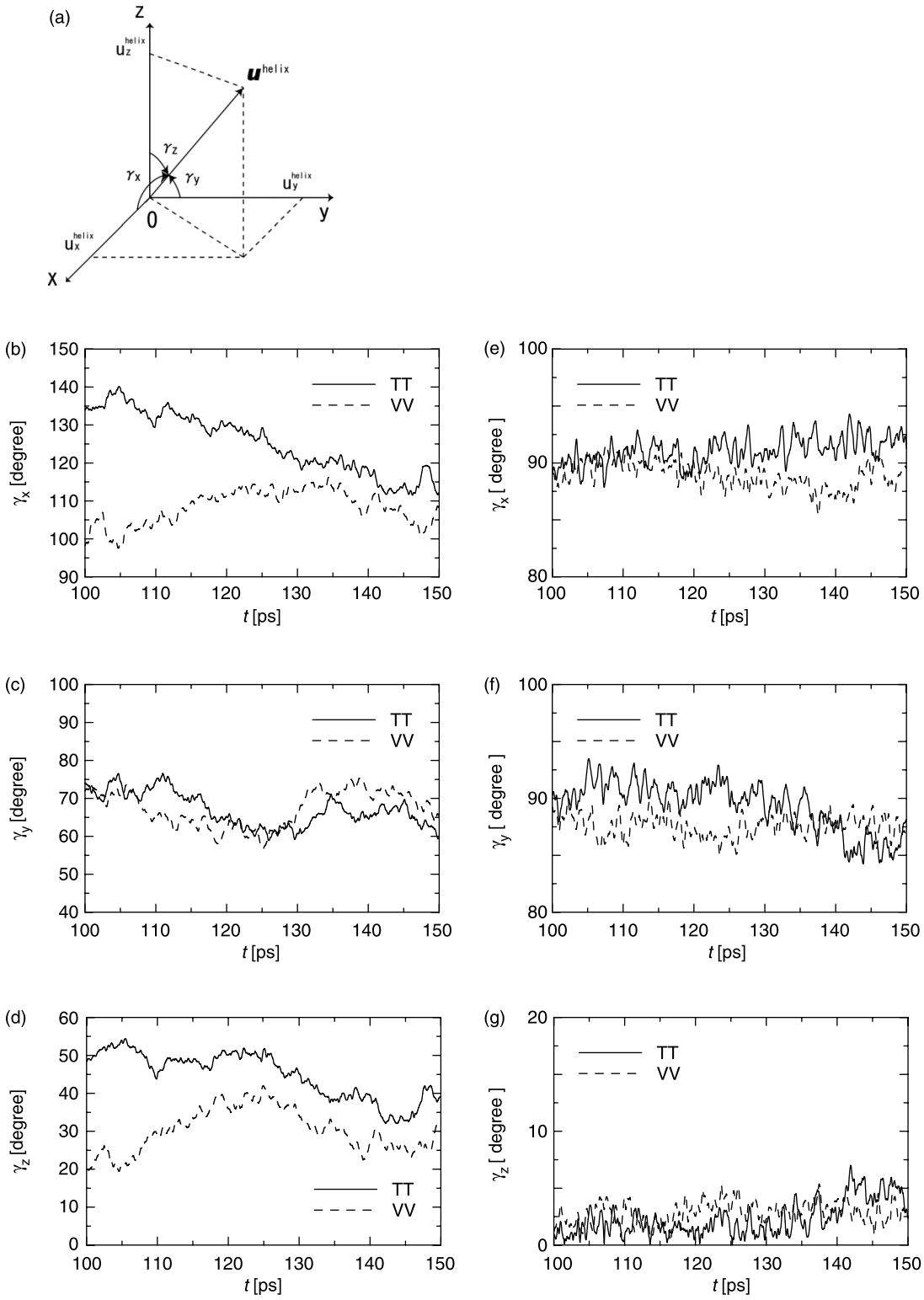

Figure 5. Time changes in the components of zenith angle: (a) definition of angles, (b) angle between the segment axis and *x*-axis at 300 K, (c) angle between the segment axis and *y*-axis at 300 K, (d) angle between the segment axis and *z*-axis at 300 K, (e) angle between the segment axis and *x*-axis at 230 K, (f) angle between the segment axis and *y*-axis at 230 K, (g) angle between the segment axis and *z*-axis at 230 K.

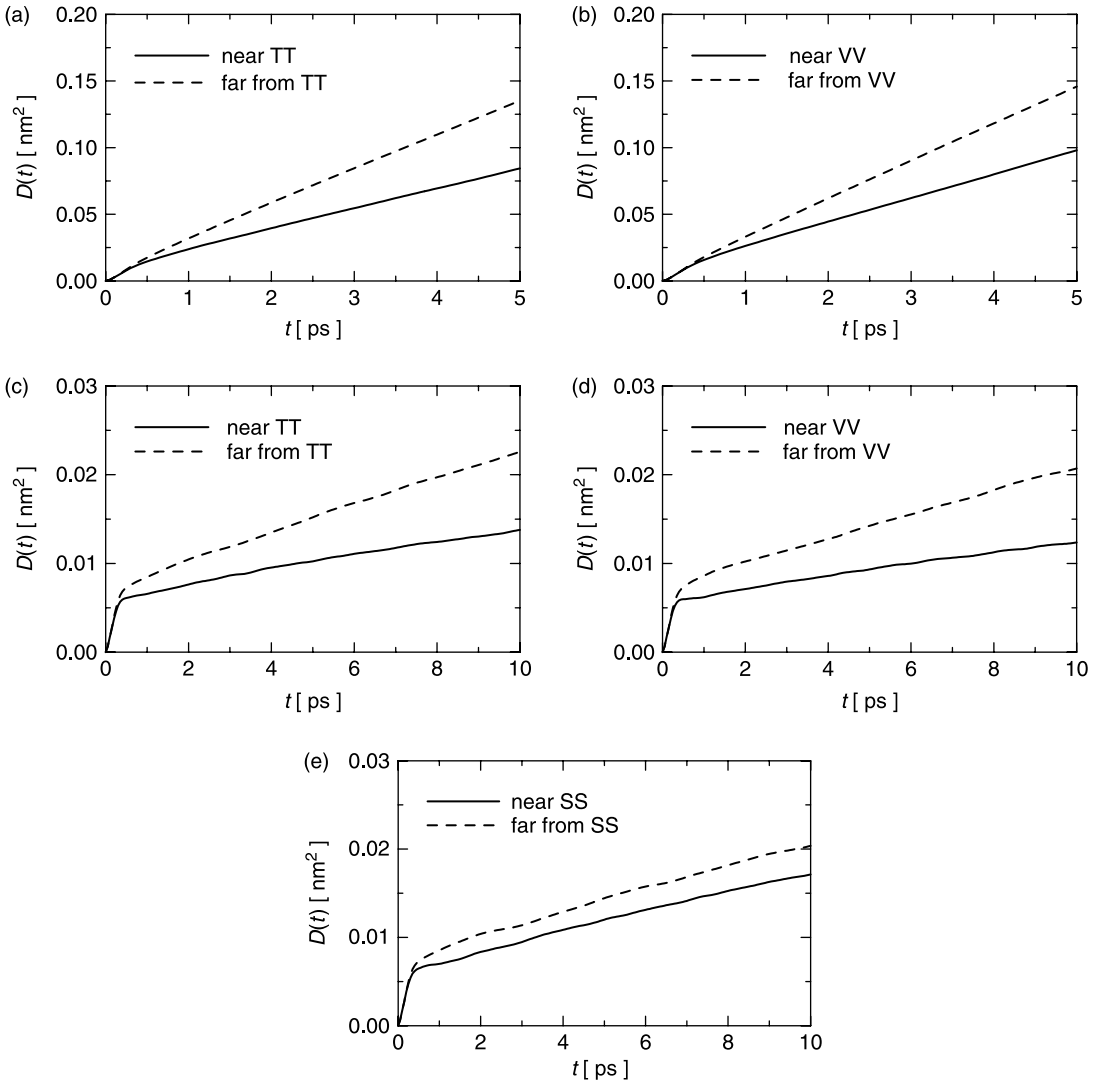

Figure 6. MSDs of water molecules: (a) in the case with the TT segment at 300 K, (b) in the case with the VV segment at 300 K, (c) in the case with the TT segment at 230 K, (d) in the case with the VV segment at 230 K, (e) in the case with the SS segment at 230 K.

$r = 0.27$ nm and $\alpha_{HB} = 106°$ in the case of the oxygen atoms. Also, peaks are seen around $r = 0.19$ nm and $\alpha_{HB} = 166°$ and $r = 0.33$ nm and $\alpha_{HB} = 60°$ in the case of the hydrogen atoms. These confirm the hydrogen bond among water molecules, which takes a tetrahedral coordination. This coordination is one of the typical coordinations of a cluster of water molecules.

4.4.2 Case 1

We focus on the hydrogen and oxygen sites of Thr24 and Asn27 in the TT segment. Figure 9(a) and (b) show the ADF of the water molecules near the oxygen site in Thr24 and the hydrogen site in the hydroxyl group in Thr24 in Case 1, respectively. Figure 9(c)–(e) show the ADF of the water molecules near the oxygen site in Asn27, the hydrogen site H_{N1} in Asn27 and the hydrogen site H_{N2} in Asn27 in Case 1, respectively. A peak is seen around $r = 0.28$ nm and $\alpha = 106°$ in the case of the oxygen site in each residue. This is in agreement with the result shown in Figure 8(a).

In contrast with this, the angles of the peaks concerning the hydrogen sites are clearly lower than those in Figure 8(b): α_{HB} is 150° in the case of the hydrogen site of Thr24, 158° in the case of the H_{N1} in Asn27 and 130° in the case of the H_{N2} in Asn27. The distance between the hydrogen site of Thr24 and that of Asn27 (H_{N2}) is 0.49 nm in the TT segment. Two water molecules can be located by the hydrogen bond near the line passing through these two hydrogen sites. The angle is 134° in this case. Thus, the peaks shown in Figure 9(b),

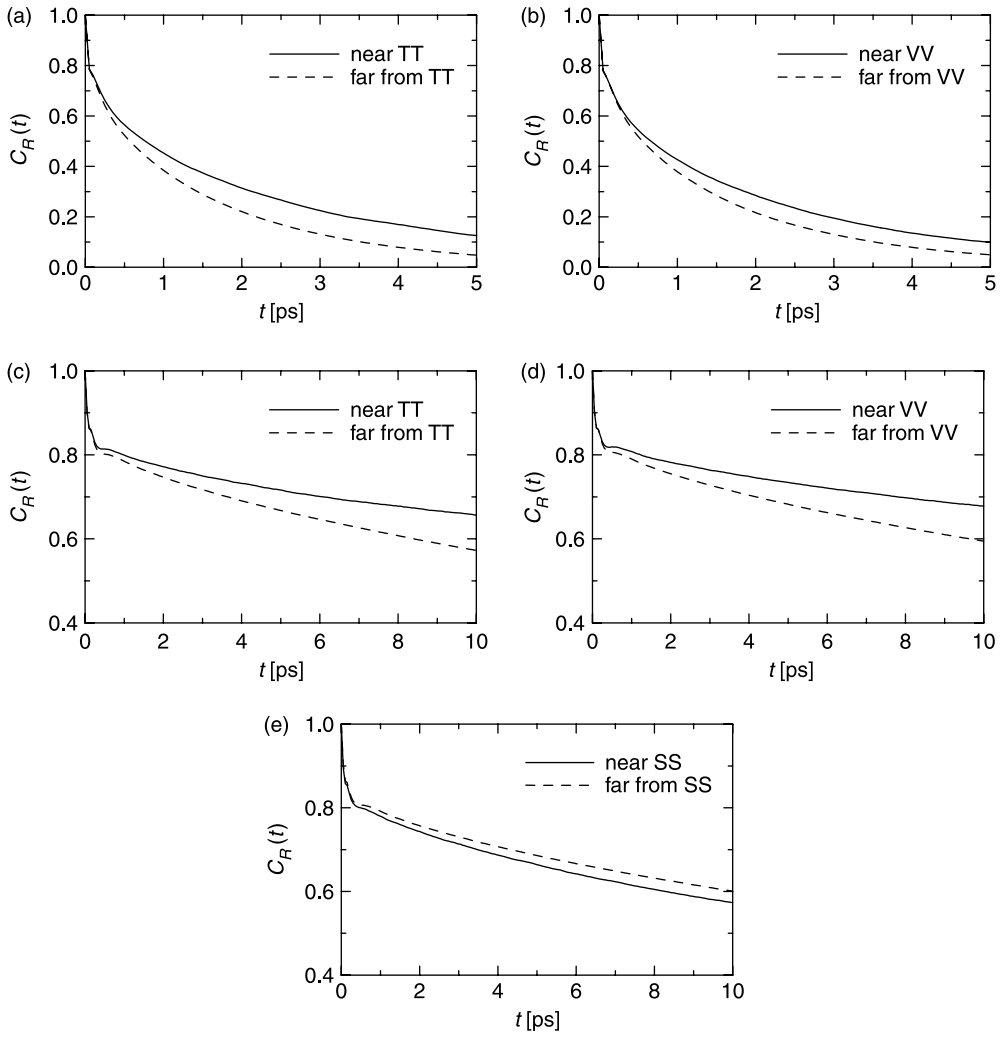

Figure 7. CFRs of water molecules: (a) in the case with the TT segment at 300 K, (b) in the case with the VV segment at 300 K, (c) in the case with the TT segment at 230 K, (d) in the case with the VV segment at 230 K, (e) in the case with the SS segment at 230 K.

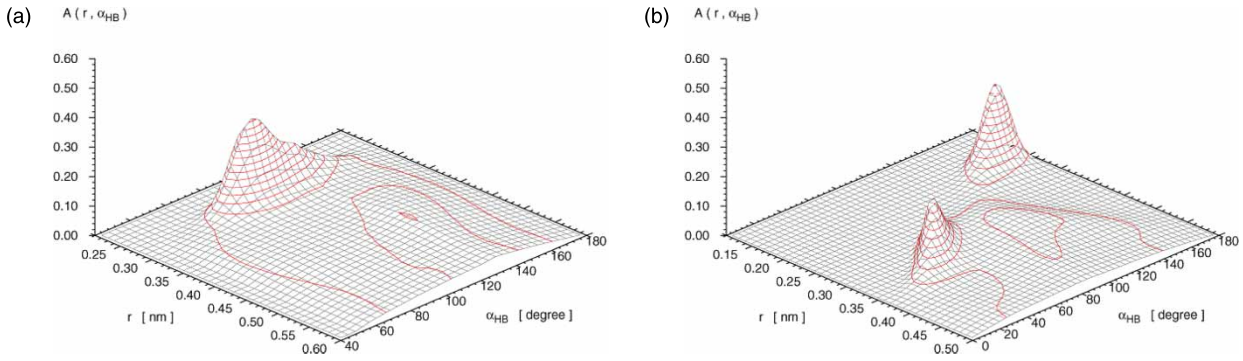

Figure 8. ADFs of water molecules at 300 K: (a) oxygen site ($O_w \cdots O_w$—$H_{w\ far}$), (b) hydrogen site (O_w—$H_w \cdots O_w$).

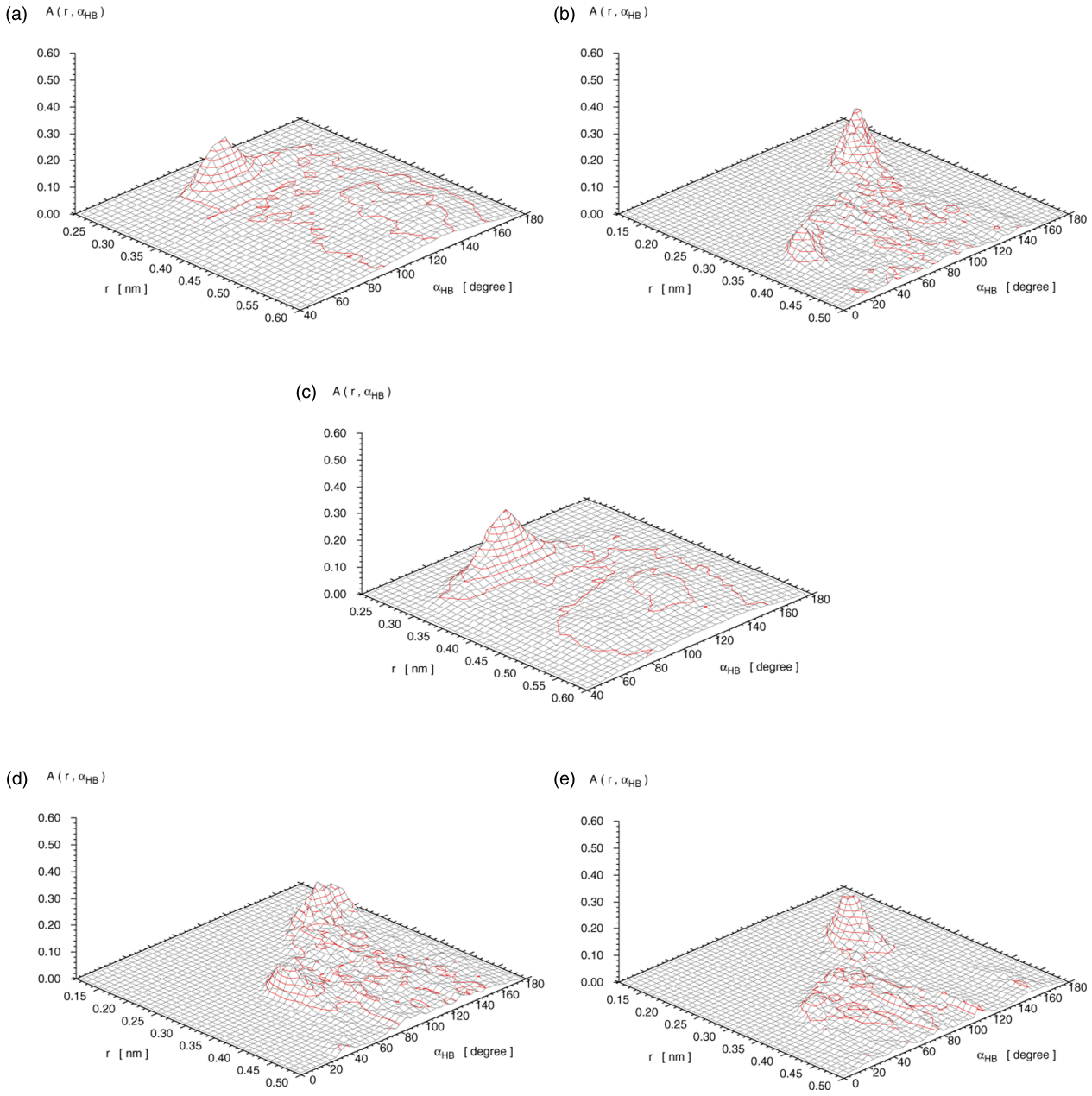

Figure 9. ADFs of sites of the TT segment at 300 K: (a) oxygen site of Thr24 (O $\cdots$ O_w—$H_{w\ far}$), (b) hydrogen site of Thr24 (O—H $\cdots$ O_w), (c) oxygen site of Asn27 (O $\cdots$ O_w—$H_{w\ far}$), (d) hydrogen site (H_{N1}) of Asn27 (N—H_{N1} $\cdots$ O_w), (e) hydrogen site (H_{N2}) of Asn27 (N—H_{N2} $\cdots$ O_w).

(d) and (e) are considered to be caused by these specific water molecules.

The angle of the peak concerning the hydrogen sites of Thr35 is 162° (figure omitted). This value is higher than that of Thr24 mentioned above. This indicates that the possibility of a hydrogen bond between water molecules and the hydrogen sites of Thr35 is lower than the possibility of the hydrogen bond mentioned above. Similarly, the angles of the peaks concerning the H_{N1} and H_{N2} in Asn27 of the VV segment are 166° and 138°, respectively (figures omitted). These values are higher than the values concerning these hydrogen sites in Asn27 of the TT segment mentioned above. This indicates that the possibility of a hydrogen bond between water molecules and the hydrogen sites of Asn27 in the VV segment is lower than the possibility of the hydrogen bond mentioned above. Therefore, the combination of Thr24 and Asn27 leads to the hydrogen bond of water

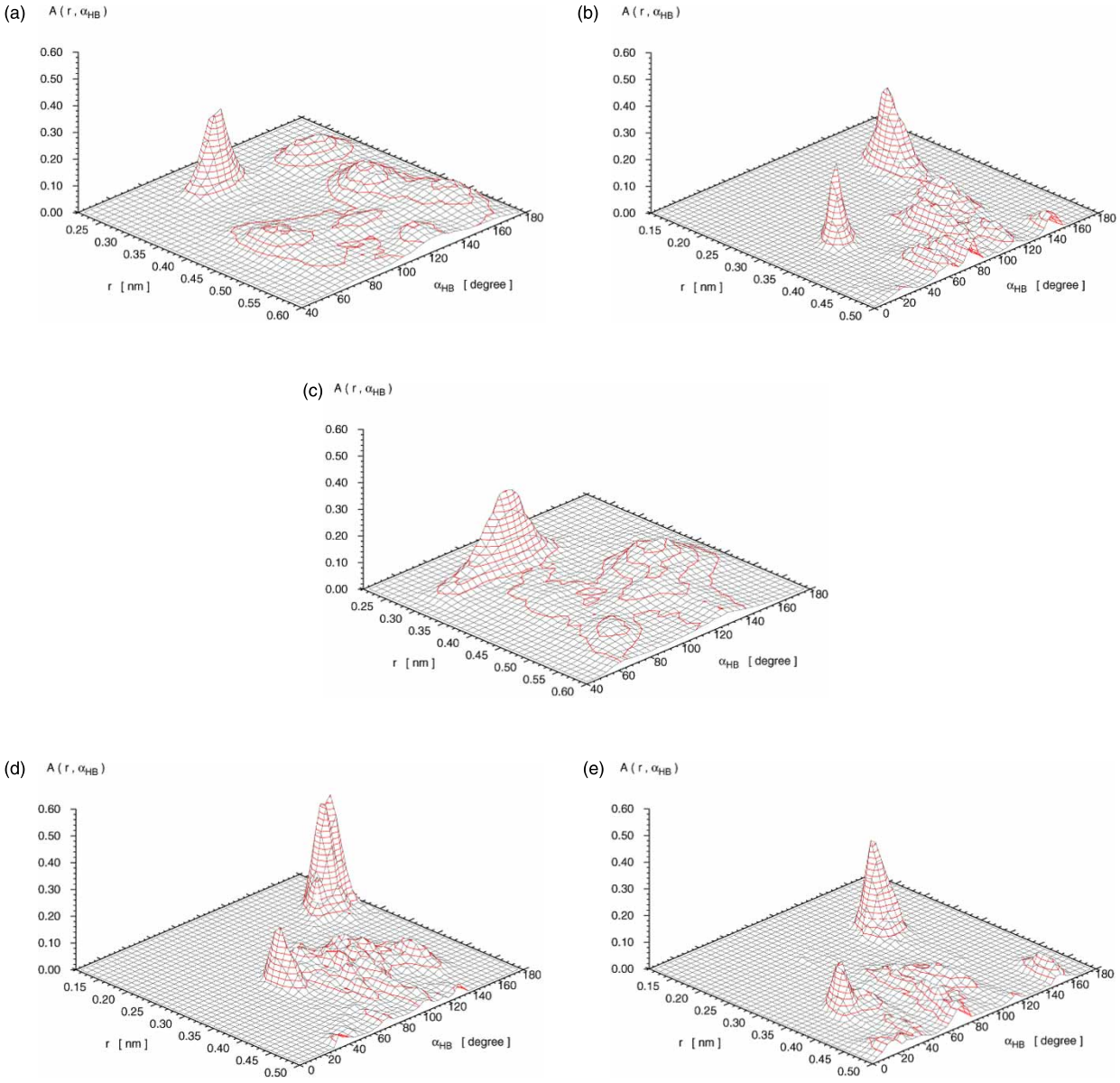

Figure 10. ADFs of sites of the TT segment at 230 K: (a) oxygen site of Thr24 ($O \cdots O_w$—$H_{w\ far}$), (b) hydrogen site of Thr24 (O—H $\cdots$ O_w), (c) oxygen site of Asn27 ($O \cdots O_w$—$H_{w\ far}$), (d) hydrogen site (H_{N1}) of Asn27 (N—$H_{N1} \cdots O_w$), (e) hydrogen site (H_{N2}) of Asn27 (N—$H_{N2} \cdots O_w$).

molecules nearby. This is consistent with the experimental results obtained by Loewen *et al*. [10].

4.4.3 Case 2

Figure 10(a) and (b) depict the ADF of the water molecules near the oxygen site in Thr24 and the hydrogen site in the hydroxyl group in Thr24 in Case 2, respectively. Figure 10(c)–(e) depict the ADF of the water molecules near the oxygen site in Asn27, the hydrogen site H_{N1} in Asn27 and the hydrogen site H_{N2} in Asn27 in Case 2, respectively. A peak in the case of the oxygen site in each residue is seen at the same location as those seen in Figures 8(a), 9(a) and (c). The angle of the peak concerning the H_{N2} of Asn27 is 130°, which is equal to that in Case 1, while the angle of the peak concerning the hydrogen sites of Thr24 is 142°, which is lower than that in Case 1. Thus, the hydrogen bond between the water molecules and these hydrogen sites is slightly more remarkable at low temperature. The angles of the peak concerning the hydrogen sites of Thr35 and H_{N2} in Asn27 of the VV segment are higher than those of the TT segment. Note that we cannot explain the low fluctuations of zenith angles in Case 2 discussed in

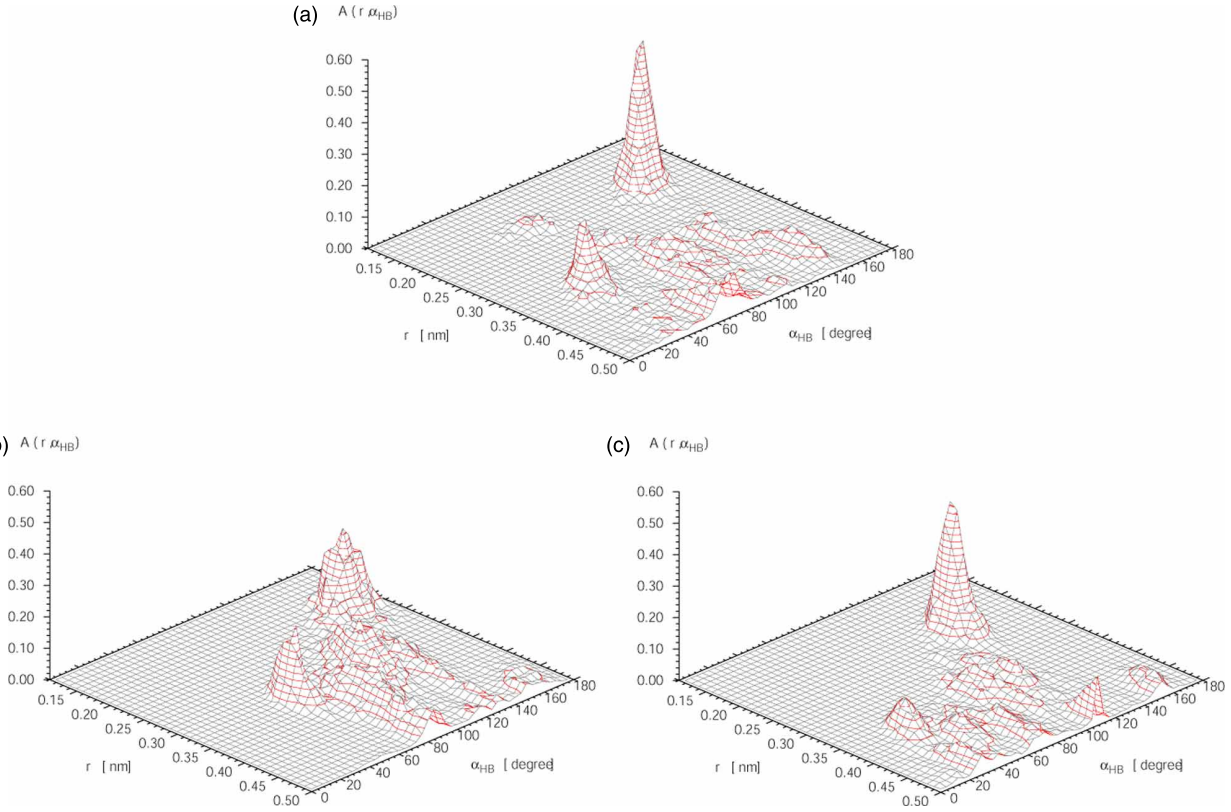

Figure 11. ADFs of sites of the SS segment at 230 K: (a) hydrogen site of Ser24 (O—H $\cdots$ O_w), (b) hydrogen site (H_{N1}) of Asn27 (N—H_{N1} $\cdots$ O_w), (c) hydrogen site (H_{N2}) of Asn27 (N—H_{N2} $\cdots$ O_w).

Section 4.1 from the results shown in Figures 9 and 10. This will be discussed later.

Figure 11(a)–(c) show the ADF of the hydrogen site of hydroxyl group in Ser24, the hydrogen site H_{N1} in Asn27 and the hydrogen site H_{N2} in Asn27 of the SS segment in Case 2, respectively. The peaks except for the highest one in Figure 11(a) are lower than those corresponding peaks in Figure 10(b), (d) and (e). This shows that the region, where the hydrogen bond occurs between the water molecules and the hydrophilic sites in the Ser24 and Asn27, spreads more widely compared with that in the TT segment. This is consistent with the results in the MSD and CFR mentioned above. It can be considered that the three hydrogen sites and one oxygen site in the serine residue attract the water molecules to each other. Thus, the water molecules move and rotate easily near the SS segment, as shown in Figures 6(e) and 7(e). This is consistent with the experimental results obtained by Zhang and Laursen [8].

4.4.4 Methyl sites

We also focus on the ADF of the water molecules near the methyl sites of alanine residues in the TT segment. Note that the following results are also obtained in the case with the VV segment. Figure 12(a) and (b) exhibit the ADF at 300 K in the case of the angle shown in Figure 3(e) and that shown in Figure 3(f), respectively. Figure 12(c) and (d) indicate the ADF at 230 K in the case of the angle shown in Figure 3(e) and that shown in Figure 3(f), respectively. Gentle peaks are seen around $r = 0.37$ nm and $\alpha_{HB} = 62°$ in Figure 12(b) and (d). The other gentle peaks are seen around $r = 0.35$ nm and $\alpha_{HB} = 72°$ and 158° in Figure 12(a) and (c). These show that the water molecules are concentrated around the methyl sites of alanine residues. This is more noticeable in Case 2 than Case 1.

4.5 Dihedral angles

Figure 13(a) and (b) show the DADF of the water molecules near the methyl site of alanine residues in the TT segment in Case 1 and Case 2, respectively. Figure 13(c) shows the DADF of all the water molecules in the case with TT segment in Case 2. The r is fixed at 0.375 nm. It is found that the distribution of the DADF in Figure 13(c) is broad with respective to the two angles. This is because the water molecules take various coordinations in the spherical region of $r < 0.375$ nm due to the hydrogen bond. In contrast with this, three peaks are clearly seen around $\beta \approx 120,\ 0,\ -120°$ for

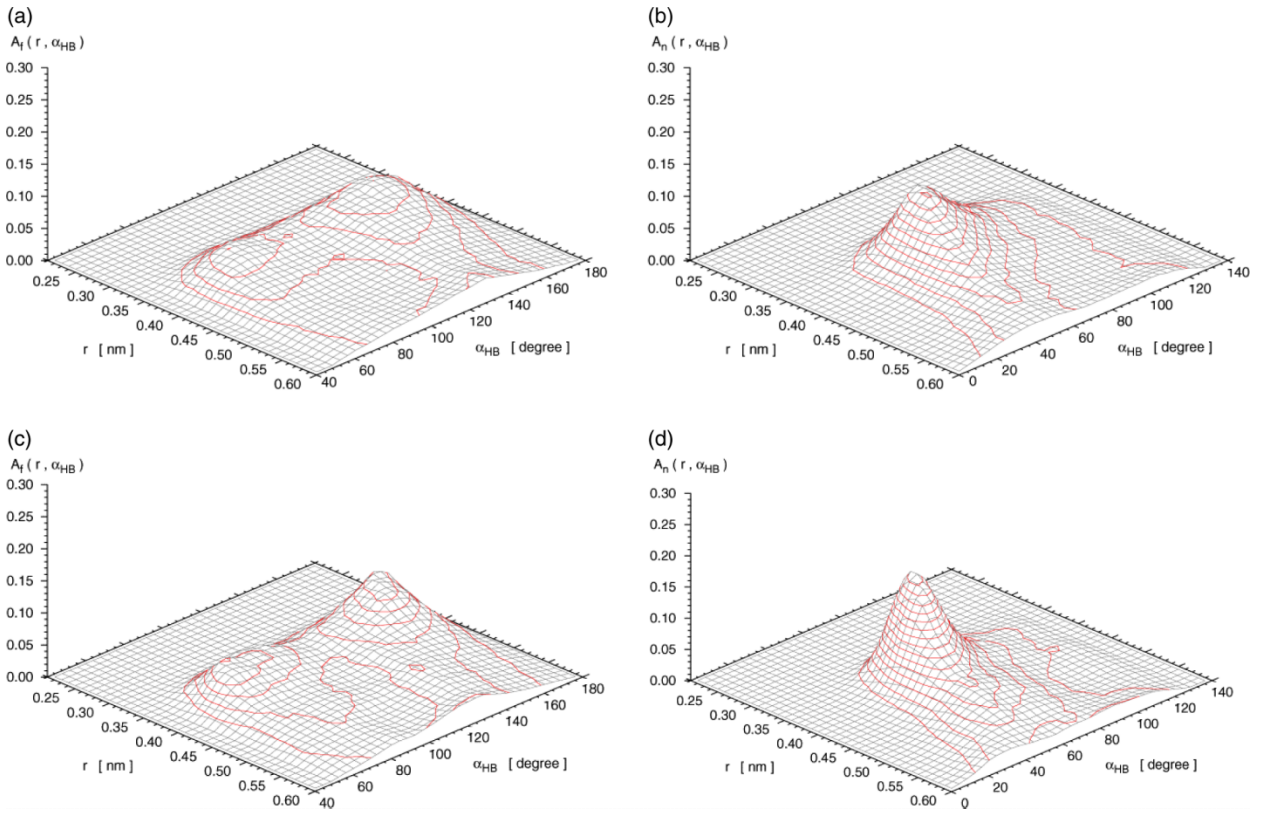

Figure 12. ADFs of water molecules near methyl sites of alanine residues of the TT segment: (a) ($CH_3 \cdots O_w$—$H_{w\ far}$) in Case 1, (b) ($CH_3 \cdots O_w$—$H_{w\ near}$) in Case 1, (c) ($CH_3 \cdots O_w$—$H_{w\ far}$) in Case 2, (d) ($CH_3 \cdots O_w$—$H_{w\ near}$) in Case 2.

$\alpha_{HB} \approx 60°$ in Figure 13(a) and (b). This means that the peaks on both sides are symmetrical in respect of $\beta = 0°$. It is thought from this result that three patterns exist in the orientation of the water molecules in the neighbourhood of the alanine residues. Since β is set equal to zero degrees when three atoms of a water molecule and the methyl site are on one plane, the symmetric represents the symmetrical orientation of the water molecules. It is found from geometrical calculations that the orientation in the case of $\beta = 0°$ corresponds to the peak at $\alpha_{HB} = 158°$ in Figure 12(a) and (c), and that the orientation in the case of $\beta = \pm 120°$ corresponds to the peak at $\alpha_{HB} = 72°$ in Figure 12(a) and (c). These facts demonstrate that the water molecules gather in the spherical shell regions, whose radius is 0.375 nm from the methyl sites of the alanine residues. It can be considered that the gathering of water molecules is due to the hydrophobic hydration around the methyl sites. This gathering occurs not only on the hydrophobic side but also on the hydrophilic side of the TT segment because three alanine residues are located on the hydrophilic side. From the comparison of the peak values shown in Figure 13, the gathering is found more predominant in Case 2 than Case 1. Thus, it is considered that the gathering of water molecules on both sides of segments is the reason for the attenuation of the zenith-angle fluctuation in Case 2.

5. Conclusions

A molecular dynamics simulation was carried out for water with the rigid TT α-helical segment, which simulated the part of AFP type I. The VV segment, in which the two threonine residues of the TT segment were replaced with valine residues, and the SS segment, in which the two threonine residues were replaced with serine residues, were also dealt with. The main conclusions obtained are as follows:

(1) The MSD, the CFR, the ADF and the DADF are effective for analysing the interaction of water molecules and the segments.
(2) The two hydrogen sites in the amino group of Asn27 and the hydrogen site of the hydroxyl group in Thr24, which are positioned close to each other, play an important role in the hydrogen bond between the water molecules and these sites. The possibility of a hydrogen bond between water molecules and the hydrogen site in Thr35 is lower than the possibility of the hydrogen bond between

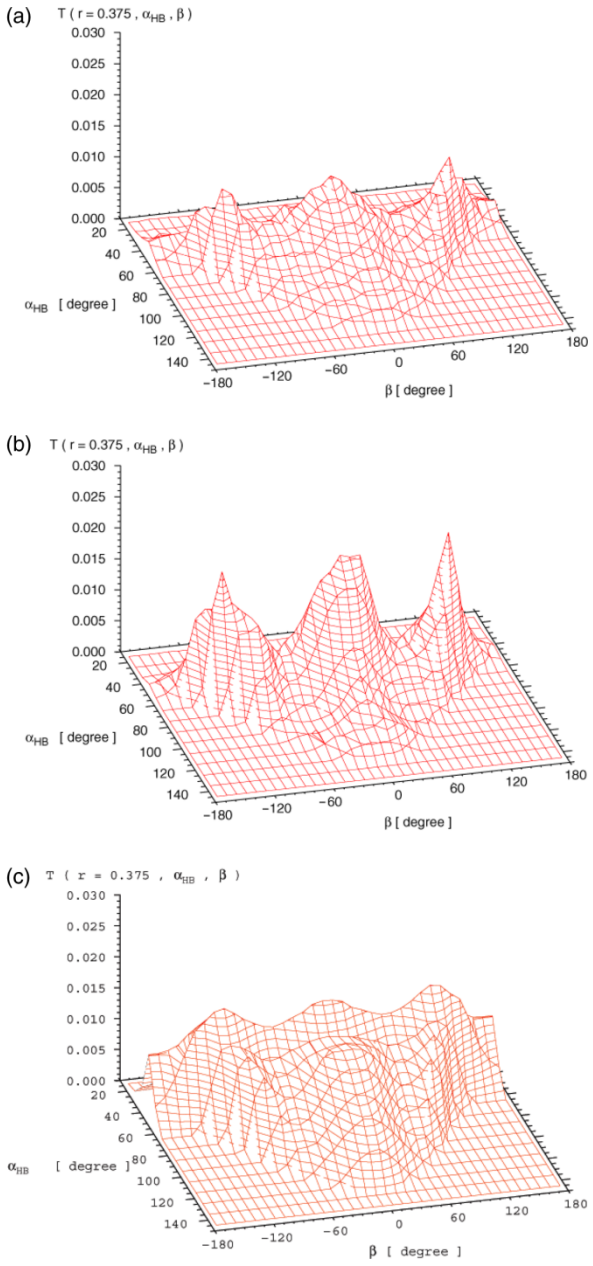

Figure 13. DADFs in the case with the TT segment: (a) for the water molecules near methyl sites of alanine residues in Case 1, (b) for the water molecules near methyl sites of alanine residues in Case 2, (c) for all the water molecules.

the water molecules and the hydrogen sites of the hydroxyl group in Thr24. This proves the importance of the hydrogen sites in Asn27. This is consistent with the experimental results obtained by Loewen *et al*. The hydrogen bond is slightly more remarkable in the case of low temperature.

(3) The possibility of a hydrogen bond between water molecules and the hydrogen site in Val24 is lower than that in Thr24. This is because the hydroxyl group in Thr24 is replaced with the methyl group in Val24.

(4) The zenith-angle fluctuation of the TT segment is more noticeable than that of the VV segment at 300 K. This is due to the hydrogen bond mentioned above. On the other hand, at 230 K, the zenith-angle fluctuations of these segments are low. This is because the gathering of water molecules around the methyl sites of alanine residues due to the hydrophobic hydration is predominant at the low temperature. The zenith-angle fluctuation is related to the approach of the segment to the ice surface. This will be discussed in our next paper.

(5) The three hydrogen sites and one oxygen site in the serine residue attract water molecules around these sites. Thus, the serine residues enhance the mobility of water molecules. This is consistent with the experimental results obtained by Zhang and Laursen.

Acknowledgements

This study was partially supported by the Ministry of Education, Culture, Sports, Science and Technology of Japan through the Grant-in-Aid for Exploratory Research (No. 16656071) and the Grant-in-Aid for Scientific Research (C) (No. 19560206). The authors also acknowledge Professor H. Urakawa at the Department of Chemistry and Materials Technology, Kyoto Institute of Technology, for his kind checking of the manuscript.

References

[1] B. Li and D.-W. Sun, *Novel methods for rapid freezing and thawing of foods – a review*, J. Food Eng. 54 (2001), p. 175.
[2] G.L. Fletcher, S.V. Goddard, and Y. Wu, *Antifreeze proteins and their genes: From basic research to business opportunity*, Chemtech 29 (1999), p. 17.
[3] G. Amir *et al*., *Improved viability and reduced apoptosis in sub-zero 21-hour preservation of transplanted rat hearts using anti-freeze proteins*, J. Heart Lung Transplant. 24 (2005), p. 1915.
[4] D.S.C. Yang *et al*., *Crystal structure of an antifreeze polypeptide and its mechanistic implications*, Nature 333 (1988), p. 232.
[5] C.A. Knight, C.C. Cheng, and A.L. DeVries, *Adsorption of alpha-helical antifreeze peptides on specific ice crystal surface planes*, Biophys. J. 59 (1991), p. 409.
[6] Y. Yeh and R.E. Feeney, *Antifreeze proteins: structures and mechanisms of function*, Chem. Rev. 96 (1996), p. 601.
[7] H. Chao *et al*., *A diminished role for hydrogen bonds in antifreeze protein binding to ice*, Biochemistry 36 (1997), p. 14652.
[8] W. Zhang and R.A. Laursen, *Structure–function relationships in a type I antifreeze polypeptide*, J. Biol. Chem. 273 (1998), p. 34806.
[9] A.D.G. Haymet, L.G. Ward, and M.M. Harding, *Winter flounder 'antifreeze' proteins: synthesis and ice growth inhibition of analogues that probe the relative importance of hydrophobic and hydrogen-bonding interactions*, J. Am. Chem. Soc. 121 (1999), p. 941.
[10] M.C. Loewen *et al*., *Alternative roles for putative ice-binding residues in type I antifreeze protein*, Biochemistry 38 (1999), p. 4743.
[11] A. Jorov, B.S. Zhorov, and D.S.C. Yang, *Theoretical study of interaction of winter flounder antifreeze protein with ice*, Protein Sci. 13 (2004), p. 1537.

[12] A. Cheng and M. Merz, *Ice-binding mechanism of winter flounder antifreeze proteins*, Biophys. J. 73 (1997), p. 2851.
[13] P. Dalal *et al*., *Hydrogen bond analysis of type 1 antifreeze protein in water and the ice/water interface*, Phys. Chem. Commun. 4 (2001), p. 32.
[14] C. Yang and K.A. Sharp, *Hydrophobic tendency of polar group hydration as a major force in type I antifreeze protein recognition*, Proteins: Struct. Funct. Bioinform. 59 (2005), p. 266.
[15] A.D.G. Haymet *et al*., *Valine substituted winter flounder 'antifreeze': Preservation of ice growth hysteresis*, FEBS Lett. 430 (1998), p. 301.
[16] R. Coger, B. Rubinsky, and G. Fletcher, *Microscopic pattern of ice crystal growth in the presence of thermal hysteresis proteins*, J. Offshore Mech. Arctic Eng. (Trans. Am. Soc. Mech. Eng.) 116 (1994), p. 173.
[17] T. Nobekawa and Y. Hagiwara, *Interaction among segments of antifreeze protein type I, or their mutants, an ice crystal and water molecules*, Mol. Simul., submitted.
[18] C.W. Gear, *Numerical Initial Value Problems in Ordinary Differential Equations*. Prentice-Hall, Englewood Cliffs, 1971.
[19] W.J. Jorgensen *et al*., *Comparison of simple potential functions for simulating liquid water*, J. Chem. Phys. 79 (1983), p. 926.
[20] D. Frenkel and B. Smit, *Understanding Molecular Simulation*, Academic Press, San Diego, 1996.
[21] L. Verlet, *Computer 'experiments' on classical fluids. II. Equilibrium correlation functions*, Phys. Rev. 165 (1968), p. 201.
[22] J.P. Ryckart, G. Ciccotti, and H.J.C. Berendsen, *Numerical integration of the Cartesian equations of motion of a system with constraints: molecular dynamics of n-alkanes*, J. Comput. Phys. 23 (1977), p. 327.
[23] W.J. Jorgensen and J. Tirado-Rives, *The OPLS potential functions for proteins: Energy minimizations for crystals of cyclic peptides and crambin*, J. Am. Chem. Soc. 110 (1988), p. 1657.
[24] A.W. Reach, *Molecular Modelling – Principles and Applications*, 2nd ed., Pearson Education Ltd, Upper Saddle River, 1996.
[25] K. Iwasaki and Y. Hagiwara, *Inhibition of ice nucleus growth in water by alanine dipeptide*, Mol. Simul. 30 (2004), p. 487.
[26] M.P. Allen and D.J. Tildesley, *Computer Simulation of Liquid*, Oxford Science, Oxford, 1987.

Appendix

We examined whether or not the velocity of water molecules is isotropic. Figure A1(a) and (b) exhibit the relative velocity distributions of the water molecules in the three directions at 300 K (Case 1) in the case with the TT segment for 40 ps and those in the case with the VV segment for 40 ps, respectively. Figure A1(c) and (d) indicate the relative velocity distributions of the supercooled water molecules (Case 2) in the three directions in the case with the TT segment and those in the case with the VV segment, respectively. The relative velocity is defined as the difference between the instantaneous velocity and its spatiotemporal mean value. The distributions are nearly identical to each other. This shows that the velocity distribution is isotropic in the two cases, regardless of temperature.

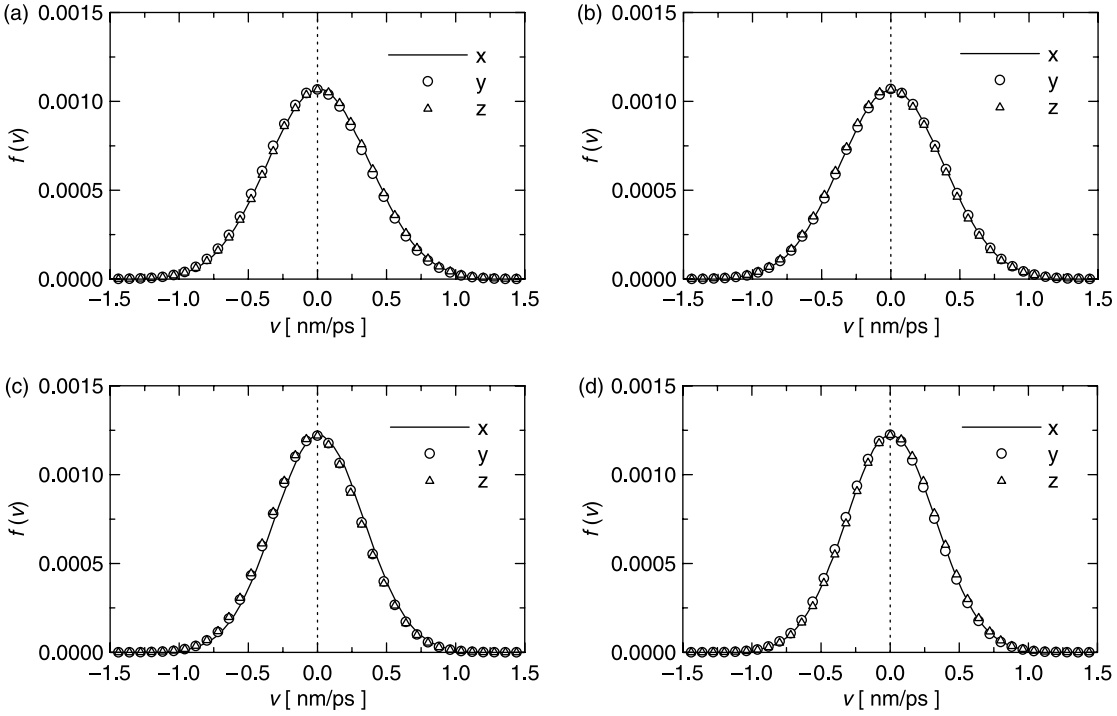

Figure A1. Velocity distributions of water molecules: (a) in the case with the TT segment at 300 K, (b) in the case with the VV segment at 300 K, (c) in the case with the TT segment at 230 K, (d) in the case with the VV segment at 230 K.